

## Schwinger variational principle calculations of wave scattering from conducting cylinders using physically motivated trial functions

B. J. Stoyanov and R. A. Farrell

*The Johns Hopkins University Applied Physics Laboratory, Johns Hopkins Road, Laurel, Maryland 20723-6099*

(Received 20 June 1995; revised manuscript received 30 August 1995)

The Schwinger variational principle for the scattering amplitude is applied to two related test problems: an infinitely long perfectly conducting circular cylinder and a hemicylindrically embossed plane illuminated by a normally incident plane wave whose magnetic field is perpendicular to the cylinder axis (TM polarization). It is demonstrated that the variational principle yields very good results with trial functions containing only a few variational parameters, provided the trial functions mimic not only the correct boundary conditions on the scatterer surface but also the expected shadowing effects of the obstacle. A variety of analytical variational limits for both low and high frequencies are derived, which, together with the numerical results for intermediate frequencies, compare very favorably with the available exact solutions.

PACS number(s): 42.25.Fx, 02.30.Wd, 03.50.De, 03.80.+r

### I. INTRODUCTION

In this paper, Schwinger's variational principle ([1–5] and pp. 1135 and 1545 of [6]) is used for plane-wave scattering from a circular cylinder and a (intimately related via the image principle [7–10]) hemicylindrically embossed plane. Applications of variational principles to virtually all kinds of problems usually lead to formidable calculations unless relatively simple expressions are utilized for trial functions [11]. Two somewhat different approaches ([12] and p. 38 of [13]) are available for designing trial functions, which lead to solutions satisfying the reciprocity theorem (p. 1131 of [6]). One approach is to represent the trial function by a linear set of basis functions and obtain the coefficients of this representation by solving the simultaneous linear equations that result from the stationary property of the scattering amplitude. The other approach consists of choosing an approximation for the field, which is physically plausible and mathematically simple, and inserting it directly into the variational expression.

With systematic methods for generating and appraising trial functions being still beyond our reach, we are led to seek trial functions which are simple and plausible rather than formal and rigorous [14]. Our procedure [15–17] is based on gaining physical insight into scattering problems for limit cases, such as very small and very large size parameters  $ka$  (product of a characteristic size of the scatterer “ $a$ ” and the wave number  $k = 2\pi/\lambda$ , where  $\lambda$  is the incident wavelength), and then to incorporate the essential physics into the trial functions. This approach can be considered as an extension of the Levine-Schwinger method [2–5] in which the variational formulation with two different approximations for the current—one in the low-frequency range and another in the high-frequency range—was used to obtain rather good results for the entire frequency range. In our approach, a single universal trial function capable of correctly reproducing both the small and large  $ka$  limits is used for the entire

frequency range.

More specifically, starting with the classic Born approximation (i.e., just the incident-wave field), we developed trial functions which not only are able to satisfy the correct boundary conditions that are known to play a key role at low and moderate frequencies [18], but are also able to approximate the basic shadowing requirements that become crucial at high frequencies (p. 1551 of [6]). One of the two adjustable parameters in the trial functions is determined by a stationary condition, while an asymptotic analysis is employed to fix the shadow-regulating parameter such that the correct large  $ka$  limit obtains for the variational forward (or specular) scattering amplitude. The adjoint trial function (pp. 1109 and 1131 of [6]), also required in the variational principle, is formulated via reciprocity which, though not mandated, is physically highly desirable because the exact field is reciprocal. In the following sections, a thorough investigation, using analytic asymptotic analyses and numerical techniques, is described for both the exact and variational results. It is demonstrated that the agreement is generally (with the exception of very rarely occurring anomalous spikes) within a few percent for all frequencies and arbitrary scattering configurations.

Although this study is concentrated on the transverse-magnetic (TM) scattering by an infinite cylinder and a hemicylindrically embossed plane, the approach itself is by no means limited to these particular scatterers, boundary condition or polarization. Thus, using similar trial fields, good accuracy was obtained for scattering from an acoustically soft (Dirichlet) sphere [15] and spheroid [16], as well as for impedance cylinders. In addition, it has been demonstrated that to obtain similar accuracy for scatterers with Neumann's boundary condition (or transverse-electric (TE) polarization), creeping-wave effects (p. 101 of [13], p. 367 of [19], and p. 217 of [20]) have to be included into the trial functions. A brief review of these and other developments, as well as additional references, can be found in [17].

## II. EXACT TM SOLUTIONS

Originally considered by Rayleigh [7], the problem of plane-wave scattering from a hemicylindrical embossment of radius "a" on an infinite perfectly conducting plane is depicted (in cross section) in Fig. 1(a). Only normal incidence is considered, and therefore the propagation vectors of both the incident and scattered waves, respectively,  $\vec{k}_i, \vec{k}_s$ , lie in a plane perpendicular to the hemicylinder axis. It is well known ([8,9] and p. 90 of [13]) that, for a perfect conductor, scattering at oblique incidence can be readily deduced from the normal-incidence solutions. The incident ( $\theta_i$ ) and scattering ( $\theta_s$ ) angles are measured from the positive x axis with counterclockwise rotations being positive. With this convention, the incident angle will be negative, so that  $-\pi \leq \theta_i \leq 0$ , while scattering angles are restricted to  $0 \leq \theta_s \leq \pi$ . The range of incident angles will be restricted to  $-\pi/2 \leq \theta_i \leq 0$ , since the results for angles between  $-\pi \leq \theta_i < -\pi/2$  are readily obtained from the symmetry of the problem. According to the Rayleigh-Tworsky image principle [7-10], this model is physically equivalent to a complete (isolated) cylinder illuminated by two plane

waves—the original incident wave and its image incident from below the (removed) base plane [see Fig. 1(b)]. Hence, the desired solution to this problem can be expressed in terms of the two complete-cylinder solutions with the angular dependence  $\phi_1 = \theta_s - \theta_i$  and  $\phi_2 = \theta_s + \theta_i$ , respectively; here  $\phi_1$  or  $\phi_2$  is the angle between the scattered-wave vector  $\vec{k}_s$  and, respectively, the incident-wave vector  $\vec{k}_i$  or its image  $\vec{k}_r$ . That is, the field scattered from the hemicylindrical embossment on the infinite plane is obtained by the superposition of the fields scattered by the full cylinder, due to the original incident wave and its image.

For a TM-polarized plane wave of unit amplitude incident at an angle  $\theta_i$  the total (incident plus scattered) scalar-wave function  $\Psi$  represents the z component of the electric field at the point  $(\rho, \theta_s)$ . From the image principle and the Dirichlet boundary condition it follows that if  $\psi$  is an isolated-cylinder wave function then

$$\Psi(\rho, \theta_s, \theta_i) = \psi(\rho, \phi_1) - \psi(\rho, \phi_2), \quad (1a)$$

and likewise for the scattering amplitudes

$$T(\theta_s, \theta_i) = t(\phi_2) - t(\phi_1), \quad (1b)$$

where

$$\phi_1 \equiv \theta_s - \theta_i, \quad \phi_2 \equiv \theta_s + \theta_i. \quad (1c)$$

The isolated cylinder scattering amplitude is given by [8,9]

$$t(\phi) = - \sum_{m=0}^{\infty} \epsilon_m \frac{J_m(ka)}{H_m^{(1)}(ka)} \cos m \phi \quad (2a)$$

with

$$\epsilon_m = \begin{cases} 1, & m = 0 \\ 2, & m = 1, 2, \dots \end{cases} \quad (2b)$$

Here  $\phi$  is the angle between the incident- and scattered-wave vectors, while  $J_m$  and  $H_m^{(1)}$  are, respectively, Bessel and Hankel functions of the first kind of order  $m$  (p. 358 of [21]). The time dependence  $e^{-i\omega t}$  is suppressed throughout and, as a rule, also suppressed are all units since our final concern is only with certain dimensionless ratios in free space.

For a subsequent comparison with the variational results, the small and large  $ka$  limits of the exact results are given next. When the frequency is sufficiently low or the radius of the cylinder is sufficiently small, so that the size parameter  $ka \ll 1$ , Eq. (2a) is approximated by

$$t(\phi) \xrightarrow{ka \ll 1} -1/C_0 - (i\pi/2)(ka)^2 \cos \phi, \quad (3a)$$

where  $C_0 \equiv 1 + (2i/\pi) \ln(\Gamma ka/2)$  with  $\ln \Gamma = \gamma = 0.57721 \dots$  being Euler's constant. Also,

$$T(\theta_s, \theta_i) \xrightarrow{ka \ll 1} -i\pi(ka)^2 \sin \theta_s \sin \theta_i. \quad (3b)$$

In the other limit, when  $ka \gg 1$ , (2a) is given by [8-10]

$$t(\phi) \xrightarrow{ka \gg 1} -\frac{1}{2} \cot \left[ \frac{\phi}{2} \right] \sin(ka \sin \phi). \quad (4a)$$

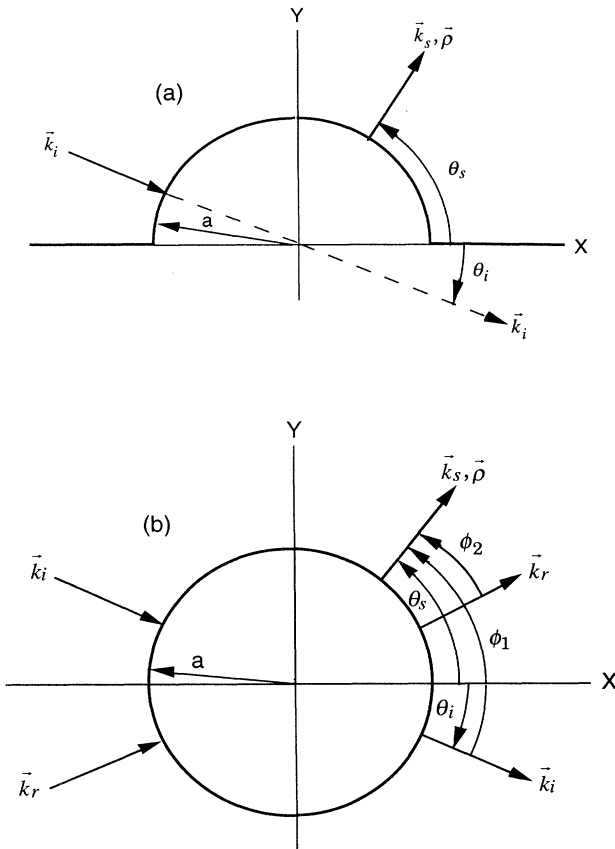


FIG. 1. Schematic representation of plane-wave scattering by a hemicylindrical embossment on a perfectly conducting plane is shown in (a). Its physical equivalent according to the image principle is depicted in (b).

This expression represents the shadow-forming part (pp. 1381 and 1551 of [6]) of the scattering amplitude, which in the forward direction ( $\phi=0$ ) has a very high "peak" yielding  $t \rightarrow -ka$  for  $ka \sin\phi \rightarrow 0$  ( $ka \gg 1$ ). The corresponding large  $ka$  limit for the hemicylinder scattering then follows directly from (4a) and (1b). Thus, for specular scattering when  $\theta_s = -\theta_i$  and  $\phi_1 = -2\theta_i, \phi_2 = 0$ , so that the observer would be in the forward direction of the image wave in the equivalent full cylinder problem [Fig. 1(b)], we get [8,9]

$$T(\theta_i) \xrightarrow{ka \gg 1} ka \left[ 1 - \frac{(\cot\theta_i)\sin(ka \sin 2\theta_i)}{2ka} \right]. \quad (4b)$$

The first term in (4b), being the shadow-forming term arising from the image wave, is the largest. The second term represents the shadow-forming term of the incident wave and is negligible except near grazing incidence  $ka \sin 2\theta_i \rightarrow 0$ , where it cancels the first term.

The normalized differential cross section is defined as (cf. p. 207 of [20])

$$\sigma = \begin{cases} |t|^2/(ka)^2 & \text{forward or specular} \\ |t|^2(4/\pi ka) & \text{otherwise} \end{cases} \quad (5)$$

for the cylinder and likewise for the hemicylinder with  $T$  substituted for  $t$ . The normalization is chosen such that  $\sigma \rightarrow 1$  for forward scattering and backscattering when  $ka \rightarrow \infty$ .

### III. VARIATIONAL FORMULATION

The standard procedure ([2-5], and pp. 1135 and 1545 of [6]) leads to the following variational expression for the (complex) scattering amplitude:

$$T^V = N\tilde{N}/D, \quad (6a)$$

where, in the usual polar coordinates and with  $-\pi/2 \leq \theta_i \leq 0, 0 \leq \theta_s \leq \pi$ ,

$$N \equiv -\frac{ia}{8} \int_0^{2\pi} d\theta' \left[ e^{-ika \cos(\theta' - \theta_s)} - e^{-ika \cos(\theta' + \theta_s)} \right] \frac{\partial \Psi(\rho', \theta')}{\partial \rho'} \Bigg|_{\rho'=a}, \quad (6b)$$

$$\tilde{N} \equiv -\frac{ia}{8} \int_0^{2\pi} d\theta \left[ e^{ika \cos(\theta - \theta_i)} - e^{ika \cos(\theta + \theta_i)} \right] \frac{\partial \tilde{\Psi}(\rho, \theta)}{\partial \rho} \Bigg|_{\rho=a}, \quad (6c)$$

$$D \equiv \frac{-ia^2}{16} \int_0^{2\pi} d\theta \int_0^{2\pi} d\theta' \left[ \frac{\partial \tilde{\Psi}(\rho, \theta)}{\partial \rho} G(\rho, \theta | \rho', \theta') \frac{\partial \Psi(\rho', \theta')}{\partial \rho'} \right] \Bigg|_{\rho'=a}. \quad (6d)$$

Here, as in the preceding section [cf. 1(a)],  $\Psi$  represents the total (incident plus scattered) field, i.e.,  $\Psi \equiv E_z$  is the electric field component along the hemicylinder axis  $z$ , and  $\hat{x} \times \nabla \Psi$  yields the remaining transverse field components. Also,  $\tilde{\Psi}$  represents the adjoint field, i.e., the solution of the reciprocal problem in which the source and observer are interchanged (p. 1135 of [6]). The adjoint trial fields are chosen such that

$$\tilde{\Psi}^{\text{trial}}(\rho, \theta; \theta_s) = \Psi^{\text{trial}}(\rho', \theta'; \theta_i) \Big|_{\theta_i = \theta_s + \pi}, \quad (7)$$

in order to have the variational solution satisfy reciprocity.

The flat-plane scalar Green's function  $G$  in (6d) can be expressed in terms of free-space two-dimensional Green's functions (p. 813 of [6]). If the correct field  $\Psi$  (and, hence,  $\tilde{\Psi}$ ) on the scatterer surface is used in (6), each of the integrals  $N$ ,  $\tilde{N}$ , and  $D$ , as well as their ratio (6a), will yield the correct scattering amplitude. However, in general, such correct surface fields are not known, which necessitates the use of approximations for  $\Psi$  (and its adjoint) on the scatterer surface to obtain an approximate variational scattering amplitude  $T^V$ .

### IV. BOUNDARY-BORN TRIAL FIELDS

Following the approach outlined in the Introduction, we start with the Rayleigh limit ( $ka \rightarrow 0$ ). A simple choice could be to employ the classic Born approximation (p. 1073 of [6]) in which the incident plane wave (including its image for the hemicylinder) is substituted for the trial field into the integrals. It turns out, however, that the resulting variational scattering amplitude for the cylinder problem  $t^V$  is incorrect even in the limit  $ka \rightarrow 0$ . Both the  $ka$  and angular dependencies are wrong in this limit [10]. On the other hand, for the hemicylinder the Born trial field provides the correct  $T^V$  in this limit [10]. To understand these results, we recall (p. 1382 of [6]) that Dirichlet's boundary condition, which requires the tangential electric field to vanish on the scattering surface, affects the wave no matter how small the radius  $a$  is compared to the incident wavelength. Obviously, the incident plane wave, by itself, cannot fit the Dirichlet boundary condition at the surface of the cylinder even in the Rayleigh limit  $ka \rightarrow 0$ . However, for the hemicylinder scattering problem the corresponding Born approximation consists of the incident plane wave and its image whose sum can easily be shown to satisfy

Dirichlet's condition for  $ka \rightarrow 0$ .

Noting that the variational principle (6) for  $T^V$  involves the value of  $\partial\Psi/\partial\rho'$  (and its adjoint) on the surface only, we need trial functions that approximate  $\partial\Psi/\partial\rho'$  on the surface  $\rho'=a$  but are quite arbitrary elsewhere. With this understanding, the classic Born-type trial fields have been amended [17] by an additional term (and its image for the hemicylinder), to get

$$\Psi^{\text{BB}}(\rho', \theta'; \theta_i) = \psi^{\text{BB}}(\rho', \varphi'_1) - \psi^{\text{BB}}(\rho', \varphi'_2), \quad (8a)$$

where the entire-cylinder trial fields are given by

$$\psi^{\text{BB}}(\rho', \varphi') = e^{ik\rho' \cos\varphi'} - f(k\rho')e^{ika \cos\varphi'}, \quad (8b)$$

with [cf. (1c)]

$$\varphi'_1 \equiv \theta' - \theta_i, \quad \varphi'_2 \equiv \theta' + \theta_i. \quad (8c)$$

The arbitrary function  $f(k\rho')$  enables the above trial fields (which we have called "boundary-Born" for obvious reasons) to satisfy Dirichlet's boundary condition

$$\psi(a, \theta') = 0, \quad (9)$$

on the cylinder surface for all values of  $ka$ , provided  $f(ka) = 1$ . The original Born-type trial fields, whose salient simplicity is largely retained in the boundary-Born trial fields, can be recovered from (8) by letting  $f(k\rho') \equiv 0$ . The quantity that enters the invariant expression for the scattering amplitude is  $\partial\Psi/\partial\rho'$  so that it will not be necessary to specify  $f(ka)$ , but only  $\partial f/\partial\rho'$  at  $\rho'=a$ . Note also that the surface current density induced by the incident plane wave and its image at the point  $(a, \theta')$  on the hemicylinder is given by (p. 37 of [20])

$$\vec{K}(a, \theta') = -\frac{\hat{z}}{i\omega\mu_0} \frac{\partial\Psi(\rho', \theta')}{\partial\rho'} \Big|_{\rho'=a} \equiv -\frac{\hat{z}}{i\omega\mu_0} \Psi'(a, \theta'), \quad (10)$$

where  $\mu_0$  is the permeability of free space.

Inserting the boundary-Born trial fields (8) and their adjoints obtained according to the prescription (7) into (6), and using Graf's addition theorem (p. 363 of [21]) at the surface of the cylinder in order to reduce the double integral in (6d) to a sum of products of two single integrals, we get

$$N = n(\phi_1) - n(\phi_2) \quad (11a)$$

and

$$D = d(\phi_1) - d(\phi_2), \quad (11b)$$

again in terms of the appropriate cylinder quantities:

$$n(\phi) = ka(i\pi/2) \left\{ \sin\frac{\phi}{2} J_1(\alpha) + J_0(\alpha) A \right\}, \quad (12a)$$

and

$$d(\phi) = k^2 a^2 (\pi^2/4) \sum_{m=0}^{\infty} \varepsilon_m \cos(m\phi) J_m(ka) H_m^{(1)}(ka) \\ \times [J'_m(ka) - J_m(ka) A] \\ \times [J'_m(ka) - J_m(ka) \tilde{A}], \quad (12b)$$

with the prime indicating that the Bessel function is differentiated with respect to its argument. Here, as in Sec. II, the angles  $\phi_1$  and  $\phi_2$  are given by (1c), while

$$\alpha = \alpha(\phi) \equiv 2ka \sin(\phi/2), \quad (13a)$$

and

$$A = \frac{1}{k} \frac{\partial f(k\rho')}{\partial\rho'} \Big|_{\rho'=0} \equiv f'(ka). \quad (13b)$$

The adjoint  $\tilde{n}$  is given by (12a) with  $A$  replaced by  $\tilde{A}$ , so that  $\tilde{n} = n$  and  $\tilde{N} = N$  provided  $\tilde{A} = A$ . According to (11), an additive image relation like (1b) holds for  $N$  and  $D$ ; however, this is not generally the case for the variational amplitude itself, i.e.,  $T^V \neq t^V(\phi_1) - t^V(\phi_2)$ , where  $t^V \neq n^2/d$ . The normalized cross sections  $\sigma^V$  are found from (5) with  $t^V$  and  $T^V$  substituted for  $t$ .

For the isolated-cylinder scattering, the as-yet arbitrary function  $A$  is treated as a variational parameter being determined through the stationary condition

$$\partial t^V / \partial A = 0. \quad (14a)$$

Generally, the variational parameter  $A$  depends not only on  $ka$  but also on the angle  $\phi$  between the incident- and scattered-wave vectors. Therefore, the stationary-evaluated  $A^{\text{cyl}}(\phi_1)$  and  $A^{\text{cyl}}(\phi_2)$  for the two entire-cylinder solutions will be different. Furthermore, the stationary  $A^{\text{hem}}(\theta_i, \theta_s)$  for the original hemicylinder problem can alternatively be deduced from

$$\partial T^V / \partial A = 0, \quad (14b)$$

with  $T^V$  given by (6a), and with  $A$  in (11)–(13) considered as a variational parameter. In general,  $A^{\text{hem}}(\theta_i, \theta_s)$  will be different from  $A^{\text{cyl}}(\phi_1)$  and  $A^{\text{cyl}}(\phi_2)$ , which will lead to different  $T^V$  values for the same  $ka$ ,  $\theta_i$ , and  $\theta_s$ . For the hemicylinder problem, we found it advantageous to treat  $A$  in (12) as the variational parameter whose stationary values are determined according to (14b). It follows from (14b) and its adjoint [and likewise from (14a)] that  $\tilde{A} = A$ , so that  $\tilde{N} = N$  (and  $\tilde{n} = n$ ).

A straightforward analytic analysis of expressions (12) for  $ka \ll 1$  shows that the agreement of  $t^V$  and  $T^V$  with the exact results holds through the higher-order terms than those given in (3). The variationally improved classic Born approximations for  $t^V$  and  $T^V$ , discussed at the beginning of this section, are recovered from the above formulas by setting  $A \equiv 0$ .

As the above analysis demonstrates, the boundary-Born trial functions are a significant improvement over the classic Born trial functions in that they produce the correct Rayleigh limits even for the entire-cylinder scattering amplitudes and cross sections for arbitrary incident and scattering directions. Moreover, by virtue of the variationally adjusted parameters  $A$ , the boundary-Born results, being extremely accurate for  $ka \lesssim 1$  (due to the correct higher-order terms beyond the lead ones), are reasonably accurate for moderate size parameters as well, as Figs. 2(a) and 3(c) illustrate for the cylinder forward ( $\phi=0$ ) and hemicylinder specular scattering at normal incidence,  $\theta_s = -\theta_i = 90^\circ$ . These results should be contrast-

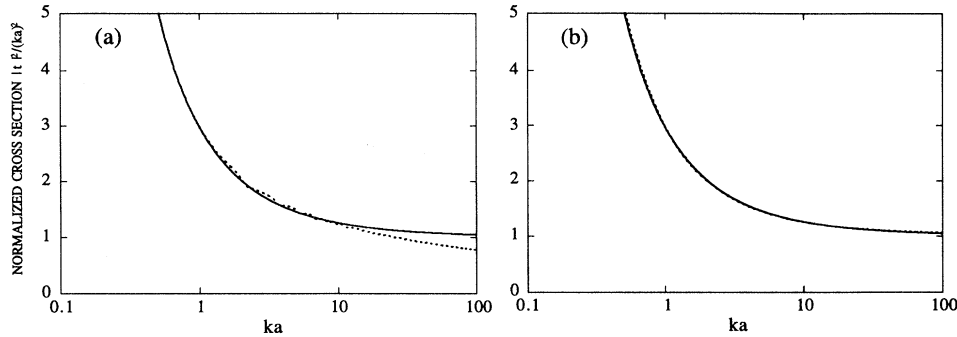


FIG. 2. Forward ( $\phi=0^\circ$ ) scattering from an isolated cylinder. The normalized variational cross sections (dashed curves) calculated by using the boundary-Born trial field without and with shadowing are compared to the exact result (solid curve) in, respectively, (a) and (b). The error at  $ka=100$  is about 26% and still increasing with  $ka$  in (a), but is less than 1.4% in (b) and will eventually disappear as  $ka \rightarrow \infty$ . The Born and Born-variational approximations for this case are identically zero and therefore not shown. The remarkable improvement achievable with physically based simple trial fields is evident.

ed to the corresponding Born (whose  $T$  is represented by  $N$  with  $A \equiv 0$ ) and Born-variational ( $A \equiv 0$ ) approximations shown for the hemicylinder problem in Figs. 3(a) and 3(b), respectively; for the isolated cylinder they are identically zero and therefore not shown. This dramatic improvement could be anticipated in view of the important role played by boundary conditions in this range of size parameters and the fact that the boundary-Born trial functions are capable of satisfying the applicable boundary conditions for all  $ka$ 's.

However, for large  $ka$  values, the variational results for the normalized cross sections appear to reproduce the correct oscillatory behavior for the hemicylinder scattering [see Fig. 3(c)], but are systematically lower than the exact results for an isolated-cylinder scattering in forward direction ( $\phi=0$ ) and for the hemicylinder scattering in specular directions ( $\theta_s = -\theta_i$ ). For these cases the error exceeds 26% at  $ka=100$  and still increases with  $ka$ , see Figs. 2(a) and 3(c). Such incorrect large  $ka$  behavior suggests that the boundary-Born trial fields, with the

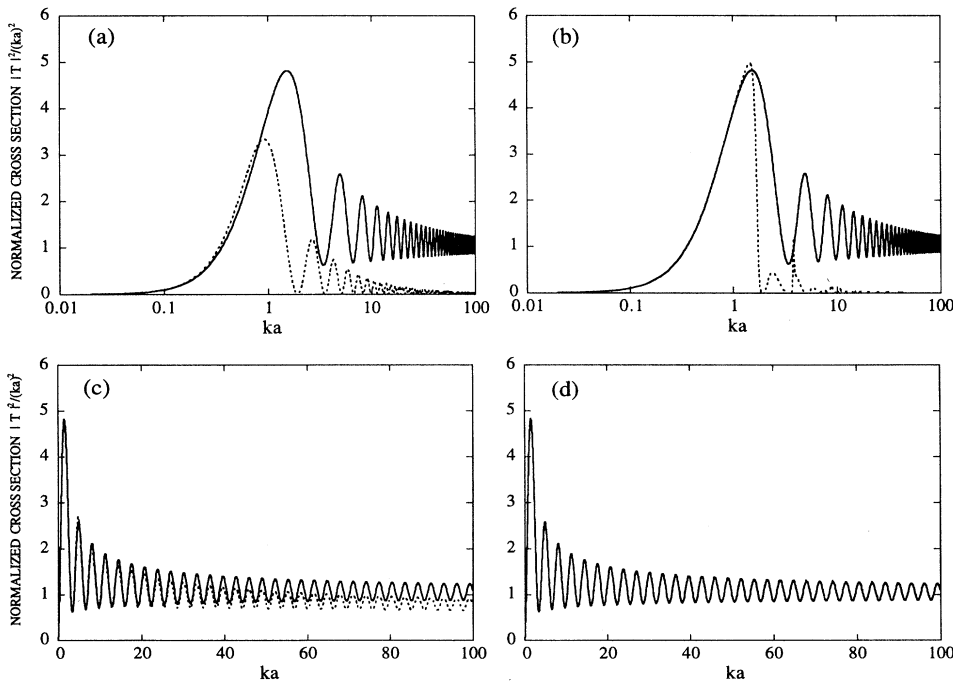


FIG. 3. Specular backscattering ( $\theta_s = -\theta_i = 90^\circ$ ) from a hemispherical embossment on an infinite plane at normal ( $\theta_i = -90^\circ$ ) incidence. The Born and Born-variational approximations (dashed curves) are compared with the exact solution (solid curve) in, respectively, (a) and (b). The variational results (dashed curves) calculated by using the boundary-Born trial field without and with shadowing are shown against the exact solution (solid curve) in, respectively, (c) and (d); a linear  $ka$  scale is used to emphasize the large  $ka$  behavior. This comparison again illustrates that all-frequency accuracy is achievable with simple trial fields.

variationally determined parameters  $A$ , may lead to incorrect asymptotic ( $ka \gg 1$ ) limits of variational results for these directions. Indeed, this inference is confirmed by an asymptotic analysis of the integrals in (6) with the trial fields defined in (8), using the results of [22]. Specifically, up to the leading terms in  $1/ka$ , the isolated-cylinder TM-scattering amplitude for forward direction is

$$t^V(\phi=0) \xrightarrow{ka \rightarrow \infty} -ka \frac{4\pi^2}{\pi^2 + 4 \ln(32\Gamma ka) - i2\pi}, \quad (15)$$

thus yielding  $t^V/ka \rightarrow 0$  logarithmically as  $ka \rightarrow \infty$ , while according to (4a) the exact  $t(\phi=0) \rightarrow -ka$  in this limit.

Thus, while the correct asymptotic ( $ka \gg 1$ ) limits for forward scattering are  $t \rightarrow -ka$  and  $\sigma \rightarrow 1$ , the variational  $t^V/ka$  and, hence,  $\sigma^V$  vanish logarithmically as  $ka \rightarrow \infty$ . Also, the same (except for the sign) leading terms hold, in the limit  $ka \rightarrow \infty$ , for the hemicylinder amplitudes in specular directions, as they should, because the observer in this case would be in the forward direction of the image wave in the equivalent full-cylinder problem, with contributions from the primary incident wave being of smaller orders in  $ka$ , cf. (4a) and (4b). Therefore, in Sec. V while further examining the above discrepancies in the asymptotic behavior of the boundary-Born variational solutions, it will be sufficient to explicitly consider analytical details only for the problem of isolated-cylinder scattering, with the extensions needed for the hemicylinder problem merely indicated.

## V. BOUNDARY-BORN TRIAL FIELDS WITH SHADOWING

The manifestly wrong asymptotic ( $ka \gg 1$ ) behavior of  $t^V$  (or  $T^V$ ) at forward (or specular) scattering indicates that the boundary-Born trial function  $\psi^{\text{BB}}$  of (8b) is lacking a significant feature which should be important for this scattering direction at large  $ka$ . According to the asymptotic expressions (4), the correct asymptotic value of the scattering amplitude for forward (or specular) scattering is due primarily to the shadow-forming wave (or its image) which produces shadowing effects through interference (pp. 1381 and 1551 of [6]) with the incident plane wave (or its image). This is by virtue of the peculiar distribution of the surface-current density  $\vec{K}$  for  $ka \gg 1$ , which approaches (p. 29 of [13], and p. 51 of [20]) twice that of the incident-wave (i.e., geometric-optics) surface current in the illuminated region, but tends to zero in the shadowed region, viz.,

$$\vec{K} \xrightarrow{ka \rightarrow \infty} \begin{cases} 2\vec{K}^{\text{inc}} & \text{illuminated} \\ 0 & \text{shadowed,} \end{cases} \quad (16a)$$

where according to the definition (10),

$$\vec{K}^{\text{inc}} \equiv -\hat{z}(k \cos\varphi' / \omega\mu_0) e^{ika \cos\varphi'}. \quad (16b)$$

The boundary-Born trial field  $\psi^{\text{BB}}$  of (8b) does not comply with this physical-optics pattern because it yields

$$\vec{K}^V \xrightarrow{ka \rightarrow \infty} \left[ 1 - \frac{2}{\pi \cos\varphi'} \right] \vec{K}^{\text{inc}}, \quad (17)$$

which has the wrong angular dependence.

Therefore, to approximate the shadowing effects in our trial field, we premultiply the original boundary-Born trial function  $\psi^{\text{BB}}$  of (8b) by a simple shadow-imitating factor, thus obtaining

$$\psi(\rho', \varphi') = (1 - \beta \cos\varphi') [e^{ik\rho' \cos\varphi'} - f(k\rho') e^{ika \cos\varphi'}], \quad (18)$$

and that for the hemicylinder follows from an additive image relation like (8a). An arbitrary (positive) parameter  $\beta$  is assumed to be independent of  $\rho'$  and  $\varphi'$ .

With these shadowed-boundary-Born trial fields, and their adjoints obtained according to (7), the variational integrals in (6) lead to the same relations (11), where now, however,

$$n = ka(i\pi/2) \left\{ \sin \frac{\phi}{2} J_1(\alpha) + i \frac{\beta}{2} [J_0(\alpha) + \cos\phi J_2(\alpha)] + A \left[ J_0(\alpha) - i\beta \sin \frac{\phi}{2} J_1(\alpha) \right] \right\} \quad (19a)$$

and

$$d = k^2 a^2 (\pi^2/4) \sum_{m=0}^{\infty} \epsilon_m \cos m\phi J_m H_m [J'_m + i\beta J''_m - A(J_m + i\beta J'_m)]^2, \quad (19b)$$

with the Bessel functions of argument  $ka$  understood in the last equation; other relevant quantities being the same as in (13). When  $\beta=0$  these expressions reduce to those obtained with the original boundary-Born trial fields without shadowing.

For forward scattering  $\phi=0$ , an asymptotic ( $ka \gg 1$ ) analysis of the variational integrals in (6), with the trial field (18), yields up to the leading term

$$t^V(\phi=0) \xrightarrow{ka \rightarrow \infty} -ka \frac{\pi^2 \beta^2}{2(4\beta^2 + \pi\beta - 2)}. \quad (20)$$

For other scattering directions asymptotic contributions to  $t^V$  are of higher orders in reciprocal powers of  $ka$ . Therefore (20), taken with the opposite overall sign, represents also the lead-term contributions to the hemicylinder-embossment scattering amplitude  $T^V$  for specular configurations when  $ka \rightarrow \infty$ .

The as-yet arbitrary parameter  $\beta$  is now adjusted so that the correct large  $ka$  limit as obtained for  $t^V$ , i.e.,  $t^V(\phi=0) \rightarrow -ka$  as  $ka \rightarrow \infty$ . This stipulation requires

$$\beta = (\pi - \sqrt{32 - 3\pi^2}) / (\pi^2 - 8) = 0.853 \dots, \quad (21)$$

the other root ( $\beta=2.507 \dots$ ) being discarded as physically inappropriate. It might seem that choosing  $\beta$  in this way restricts the applicability of this procedure to problems where the exact solution is known; however, all that is actually needed is the large  $ka$  limit of the exact solution for forward scattering, which can be obtained from the Kirchhoff (physical-optics) approximation.

The surface-current distribution resulting from (18)

and (21) has certain qualitative features that one expects from physical optics. According to (10), the surface-current density at very large size parameters is

$$\vec{K}^V \xrightarrow{ka \rightarrow \infty} (1 - \beta \cos \varphi') \vec{K}^{\text{inc}}, \quad (22)$$

with the shadow-imitating factor varying from about 0.15 for  $\varphi' = 0$  to 1.85 for  $\varphi' = \pi$ . Thus, the simple shadowing introduced in (18) leads to an approximate agreement with distribution (16), but is physically more plausible (particularly for small and moderate  $ka$ 's) than the familiar geometric shadowing in the Kirchhoff approximation used in the earlier variational work [23,24]. Geometric shadowing becomes valid only in the limit  $ka \rightarrow \infty$ , and sometimes leads to variational divergencies [25] due to the current discontinuity at the shadow boundary.

The corresponding small  $ka$  limit of the variational scattering amplitude is now approximated by the leading term as

$$t^V \xrightarrow{ka \rightarrow 0} - \left\{ C_0 - \frac{i}{2\pi} \frac{\beta^4 \cos 2\phi}{\left[ 2\beta^4 - \beta^2 \left( 8 + \frac{\cos 2\phi}{\cos \phi} \right) + 8 \right]} \right\}^{-1}. \quad (23)$$

Due to the presence of the  $\beta$ -dependent term, the agreement with the correct limit (3a) is now not as good as it was with the original boundary-Born trial function. Still, the leading term in (23) is correct, so the agreement improves as  $ka \rightarrow 0$ , independently of  $\beta$  and  $\phi$ . Also, the correct small  $ka$  limit, (3b), obtains for  $T^V$ , as can be verified using (11) and the series expansions for  $n$  and  $d$  of (19).

Thus, the boundary-Born trial fields with the properly adjusted shadowing ensure the correct small and large  $ka$  limits of the forward and/or specular scattering amplitudes. The corresponding normalized cross sections for the cylinder forward scattering and hemicylindrical-embossment specular scattering at normal incidence are shown in Figs. 2(b) and 3(d), respectively. The variational and exact results are very close for  $ka \lesssim 1$  and are in excellent agreement for large size parameters, where a slight error of less than 2% will eventually disappear since the correct leading terms are guaranteed for both  $ka \rightarrow 0$  and  $ka \rightarrow \infty$ . The largest error (of about 5%) occurs, for the hemicylinder scattering, in the intermediate region at  $ka \cong 4.8$ ; outside of this region the error is generally much less than that. To some extent, this could be anticipated since the main physical features, such as the boundary conditions and shadowing, have been properly, even if approximately, incorporated into our trial fields. Besides, the next order effects, like creeping-wave contributions (p. 101 of [13], and p. 217 of [20]), are numerically insignificant for TM scattering (p. 371 of [19]), as is apparent from the absence of any highly developed oscillatory structure in the exact cross section for the cylinder backscatter.

It is especially gratifying to have such accurate varia-

tional results (for all size parameters) for forward and/or specular directions in view of the so-called optical theorem [2-5,23] which relates the total scattering cross section to the forward and/or specular scattering amplitudes. This allows one to easily find the total cross section without carrying out the angular integration which may be quite tedious. For example, for cylinder scattering the exact total cross section is given by (p. 8 of [13])

$$\sigma_{\text{tot}} = -\frac{4}{k} \text{Ret}(\phi=0), \quad (24)$$

with the scattering amplitude represented by (2a). For the variational solution, it then follows from (23) that, up to the dominant term,

$$\sigma_{\text{tot}}^V \xrightarrow{ka \rightarrow 0} \frac{\pi^2}{k (\ln ka)^2}, \quad (25)$$

which agrees with the exact result and coincides with  $\sigma^V$  obtained through (5), since it is angular independent to this order. On the other hand, from (20) and (21), we get

$$\sigma_{\text{tot}}^V \xrightarrow{ka \rightarrow \infty} 4a, \quad (26)$$

which correctly represents the high-frequency lead term of the total cross section and is just twice the geometrical width of the cylinder, as it should be (p. 1381 of [6]).

Up to this point our analysis was mainly concentrated on the forward and/or specular scattering. We turn now to scattering at an arbitrary angle and to backscatter in particular, since this is of prime interest in monostatic radar measurements (p. 9 of [20]). As the foregoing analysis demonstrated, the original boundary-Born trial functions (without shadowing) provide excellent results for  $ka \lesssim 1$  for both cylinder and hemicylinder scattering. For moderate and large size parameters they yield backscatter cross sections that have correct average behavior, but are heavily contaminated by narrow-band spurious spikes beginning with  $ka$  somewhat larger than 1, as illustrated in Figs. 4(c) and 5(c). Again, these results are a marked improvement on the corresponding Born and Born-variational approximations shown in Figs. 4(a), 5(a), and 4(b), 5(b), respectively.

It should also be noted that the forward-scattering cross section for an isolated cylinder obtained using the original boundary-Born trial function (8b) exhibits broad wiggles of relatively small amplitudes when  $ka > 1$ . As  $ka$  increases, these anomalous wiggles become narrower and smaller, eventually turning into the ripple. The extra factor of  $ka$  in the normalization (5) for this direction reduces the apparent amplitude of the wiggles [see Fig. 2(a)]. Anomalous features in the hemicylinder specular cross section [Fig. 3(c)] arise from both the forward ( $\phi_2 = 0$ ) and backward ( $\phi_1 = 180^\circ$ ) cylinder constituents, but contributions from the latter constituent, in addition to being suppressed by the normalization, are of higher order in inverse powers of  $ka$  for  $ka \gg 1$ .

For backscatter, the shadowed-boundary-Born trial field (18) with  $\beta$  fixed by (21) yields variational results that are very accurate at all frequencies, as Figs. 4(d) and 5(d) illustrate for both the cylinder and hemicylinder scattering, respectively. For an arbitrary scattering angle

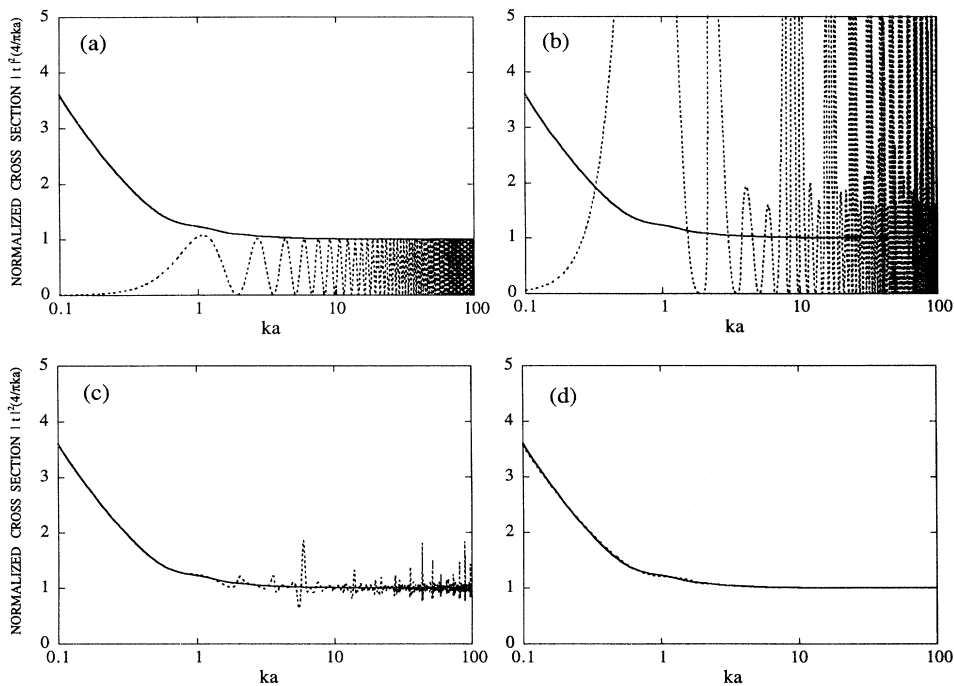


FIG. 4. Full-cylinder backscatter ( $\phi=180^\circ$ ). The designation of curves is the same as in Fig. 3. In (d) the maximum error of less than 2.5% occurs at  $ka \approx 1.5$ .

different from forward and/or specular and backscatter configurations, it is exceptionally rare that a spurious spike still persists, as Fig. 6(b) reveals for the hemicylinder cross section at  $\theta_i = -45^\circ$ ,  $\theta_s = 60^\circ$  (or, equivalently, at  $\theta_i = -60^\circ$ ,  $\theta_s = 45^\circ$  because of reciprocity and symmetry of the problem). It is interesting to note that one of the corresponding isolated-cylinder com-

ponents, namely, that with  $\phi_2 = \theta_s + \theta_i = 15^\circ$  [see 1(d)], displays a similar spike in its cross section [see Fig. 7(b)], but at a different  $ka$  location. This could be anticipated since, as pointed out earlier, the stationary parameters  $A$  are generally different for the hemicylinder and its cylinder constituents, whose respective scattering amplitudes and cross sections do not generally fit an additive

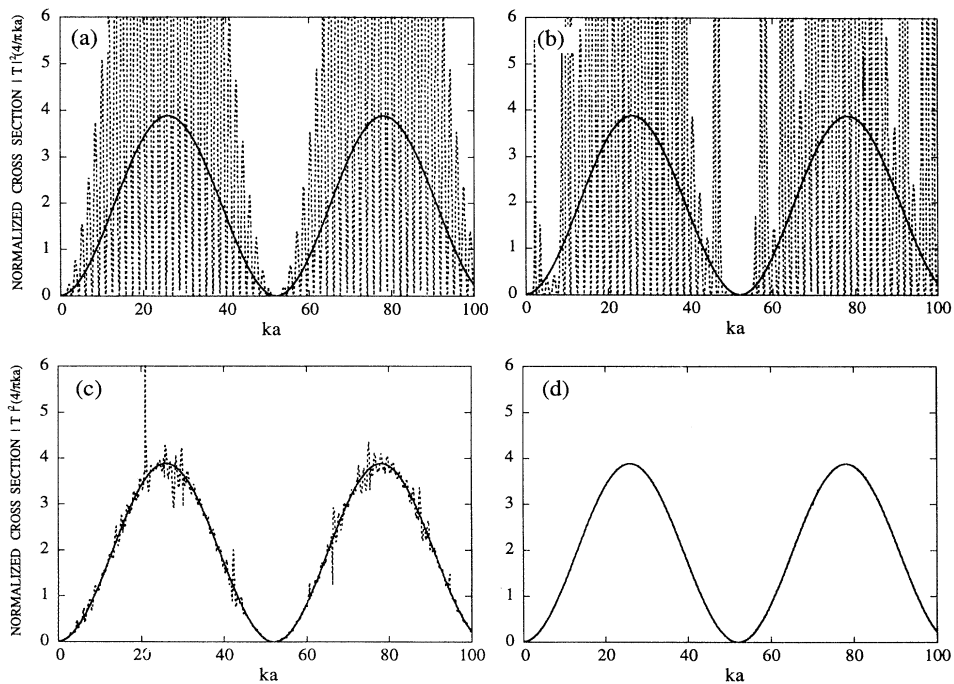


FIG. 5. Nonspecular backscatter at  $\theta_i = -20^\circ$ ,  $\theta_s = 160^\circ$  for the hemicylindrical embossment. The designation of curves is the same as in Fig. 3. Again, all-frequency accuracy is achieved.

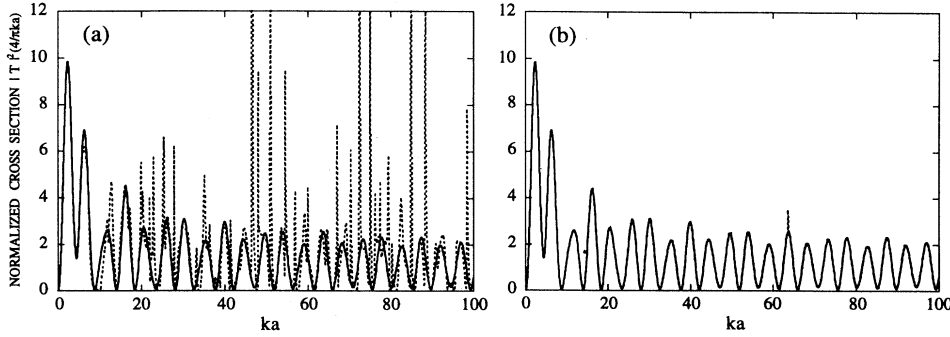


FIG. 6. Nonspecular bistatic scattering at  $\theta_i = -45^\circ$ ,  $\theta_s = 60^\circ$  from the hemicylindrical embossment. The designation of curves is the same as in Fig. 2. Notice that all spurious spikes (except one at  $ka \approx 64$ ) have disappeared in (b), and all-frequency accuracy obtains.

image relation [cf. (8a) and ff (13b)]. We also found that replacing  $\beta = 0.853 \dots$  by a simple, physically plausible  $\beta = 1$  shifts or even suppresses the remaining spurious spikes, with only marginal changes elsewhere. This fact could be used as a means to identify such spurious spikes in cases where exact solutions are unavailable.

Finally, it is worthwhile to note that the high-frequency variational formula for the normalized total cross section obtained by Papas [23] for a TM isolated-cylinder scattering using Kirchhoff's approximation, yields the correct leading term,  $\sigma_{\text{tot}}^V/4a \rightarrow 1$ , in the optical limit  $ka \rightarrow \infty$  [cf. (26)]. However, his formula does not provide adequate correction terms for large  $ka$ , which terms appear to depend on the more or less arbitrary choice of a parameter introduced in [23]. Kodis [24] derived a more accurate result for the TM cylinder total cross section, again using the Kirchhoff current distribution, but with the much more involved second [3] variational principle. His result includes the leading term plus the first correction term,  $0.746(ka)^{-2/3}$ , which has the right sign and the right frequency dependence, but whose magnitude is in error by about 50%. This produces an overall error in the normalized total cross section of about 2% or less for  $ka > 40$ .

In our asymptotic ( $ka \gg 1$ ) analysis of the variational results obtained with the original and/or shadowed-boundary-Born trial fields, only the lead terms have been provided. To derive the explicit representations of the forward and specular scattering amplitudes, and hence of the total cross sections, in reciprocal powers of  $ka$ , a more elaborate asymptotic analysis is required. However, the first correction term for  $\sigma_{\text{tot}}^V$  can be fairly easily deduced to be approximately  $0.073/(\ln ka)$ , which, although rather small for large  $ka$ , has a wrong  $ka$  dependence. Nevertheless, excellent numerical accuracy, comparable to that of Kodis's high-frequency results at  $ka \sim 40$ , was obtained for TM scattering from both a circular cylinder and a hemicylindrically embossed plane, not only for large  $ka$  and forward or specular directions, but for all size parameters and scattering configurations.

## VI. SUMMARY

Utilizing the proposed approach to develop physically plausible trial fields as a guiding principle, efficient, yet simple, trial functions have been devised, which provide all-frequency-accurate variational results for the scattering amplitudes and cross sections for TM scattering from

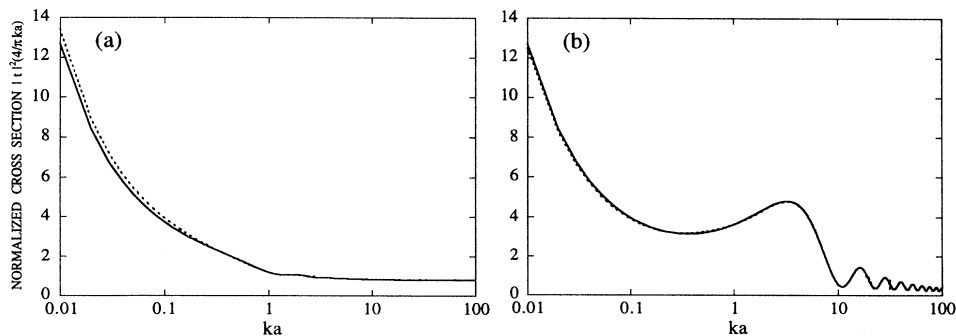


FIG. 7. The exact (solid curves) and variational (dashed curves) full-cylinder contributions [ $\phi_1 = 105^\circ$  in (a) and  $\phi_2 = 15^\circ$  in (b)] to the hemicylindrical embossment scattering shown in Fig. 6. The variational results are calculated by using the boundary-Born trial field with shadowing. The only spurious spike (at  $ka \approx 31.3$ ) in (b) corresponds to the one in 6(b). The error of about 5% at small  $ka$  in (a) will fade away as  $ka \rightarrow 0$ .

perfectly conducting infinitely long cylinders and hemicylindrically embossed planes. This was achieved by ascertaining and approximately incorporating into the trial fields the essential generic features which play physically important roles in the scattering process, using the classic Born approximation as a "seed." The significance of the boundary conditions at low and moderate frequencies is emphasized and the importance of the trial fields to be capable of satisfying these conditions is reaffirmed. The key role played by shadowing at large  $ka$  has been recognized and shadow effects have been incorporated into the trial fields. A remarkable agreement with the exact results for all size parameters has been attained for

forward and/or specular and backward scattering using the shadowed-boundary-Born trial fields that are able to satisfy the relevant boundary conditions and also contain a simple shadow-imitating factor. For other arbitrary-angle configurations an isolated spurious spike arises in very rare occasions, the accuracy elsewhere being excellent.

#### ACKNOWLEDGMENTS

We thank S. Favin for his help with numerical computations. This work was supported in part by the Navy and the National Eye Institute.

- 
- [1] J. Schwinger, *Phys. Rev.* **72**, 742 (1947).
  - [2] H. Levine and J. Schwinger, *Phys. Rev.* **74**, 958 (1948).
  - [3] H. Levine and J. Schwinger, *Phys. Rev.* **75**, 1608 (1949).
  - [4] H. Levine and J. Schwinger, *Commun. Pure Appl. Math.* **3**, 355 (1950).
  - [5] H. Levine, *Variational Methods for Solving Electromagnetic Boundary Value Problems, Notes of Lectures* (Sylvania Products Co., Mountain View, CA, 1954).
  - [6] P. M. Morse and H. Feshbach, *Methods of Theoretical Physics* (McGraw-Hill, New York, 1953).
  - [7] Lord Rayleigh, *Philos. Mag.* **14**, 350 (1907).
  - [8] V. Twersky, *IRE Trans. Antennas Propagat.* **AP-5**, 81 (1957).
  - [9] V. Twersky, *J. Acoust. Soc. Am.* **29**, 209 (1957).
  - [10] J. F. Bird, *J. Opt. Soc. Am. A* **2**, 945 (1985).
  - [11] E. Gerjuoy, A. R. P. Rau, and L. Spruch, *Rev. Mod. Phys.* **55**, 725 (1983).
  - [12] D. S. Jones, *IRE Trans. Antennas. Propaga.* **AP-4**, 297 (1956).
  - [13] *Electromagnetic and Acoustic Scattering by Simple Shapes*, edited by J. J. Bowman, T. B. A. Senior, P. L. E. Uslenghi, revised printing (Hemisphere, New York, 1987).
  - [14] M. R. Feinsein and R. A. Farrell, *J. Opt. Soc. Am.* **72**, 223 (1982).
  - [15] D. E. Freund and R. A. Farrell, *J. Acoust. Soc. Am.* **87**, 1847 (1990).
  - [16] D. E. Freund and R. A. Farrell, *J. Acoust. Soc. Am.* **89** (part 2), 1994 (1991).
  - [17] R. A. Farrell *et al.*, The Johns Hopkins University Applied Physics Laboratory Technical Memorandum No. TG 1388, 1994 (unpublished).
  - [18] D. T. Thomas, *IEEE Trans. Microwave Theory Tech.* **MTT-17**, 447 (1969).
  - [19] H. C. van de Hulst, *Light Scattering by Small Particles* (Dover, New York, 1981).
  - [20] *Radar Cross Section Handbook*, edited by G. T. Ruck (Plenum, New York, 1970).
  - [21] *Handbook of Mathematical Functions*, edited by M. Abramowitz and I. A. Stegun (Dover, New York, 1972).
  - [22] B. J. Stoyanov, R. A. Farrell, and J. F. Bird, *J. Comp. Appl. Math.* **50**, 533 (1994).
  - [23] C. H. Papas, *J. Appl. Phys.* **21**, 318 (1950).
  - [24] R. D. Kodis, *Proc. Camb. Philos. Soc.* **54**, 512 (1958).
  - [25] J. F. Bird, *J. Opt. Soc. Am. A* **3**, 2047 (1986).